Chapter 4

Relativistic Anharmonic Cyclotron Oscillator

An electron in a uniform magnetic field moves in a familiar circular cyclotron orbit [74, 30]. The complete quantum mechanical treatment using the Dirac equation is discussed in [11]. The motion of an electron of charge $-e$ and mass m in a uniform magnetic field $\mathbf{B}$ is governed by the Lorentz force law,

$$d(m\mathbf{v})/dt = -(e/c)\mathbf{v} \times \mathbf{B} - e\mathbf{E} + \mathbf{F}_r. \tag{4.1}$$

The term $\mathbf{F}_r$ is due to radiation damping. The motion is in a circle with a frequency

$$2\pi\nu_c = \omega_c = \frac{eB}{\gamma mc}, \tag{4.2}$$

where γ is the familiar relativistic factor, $\gamma = 1/\sqrt{1-(\frac{v}{c})^2}$. The cyclotron orbit has radius

$$r_c = \frac{c\sqrt{2\mathrm{E}_c m}}{eB}, \tag{4.3}$$

where E_c is the kinetic energy of the motion. This cyclotron motion of an electron is slightly modified by the electrostatic potential of the Penning trap, and is typically at a high microwave frequency of about 150 GHz, with a wavelength of 2 mm. The

motion is brought to thermal equilibrium with the 4 K environment by synchrotron radiation with a damping rate given by

$$\gamma_c = \frac{4r_0\omega_c^2}{3c} \tag{4.4}$$

where $r_0 \simeq 2.8 \times 10^{-13}$ cm is the classical electron radius and c is the speed of light. At 5.3 Tesla the damping time is $\gamma_c^{-1} \simeq 10^{-1}$ sec. This spontaneous emission rate can be either enhanced or inhibited by the environment [38]. The coarse energy level structure is that of a harmonic oscillator ladder (known as Landau levels), with a separate ladder for each value of the electron spin. (See also [19].) Relativistic corrections make the oscillator slightly anharmonic [56, 39], as can be seen from Eq. 4.2. In other words, the electron and electromagnetic field system is intrinsically nonlinear [55] without depending on macroscopic nonlinear properties of a medium. This anharmonicity is often identified as a relativistic mass increase,

$$m = \gamma m_0 = (1 + K/mc^2)m_0, \tag{4.5}$$

where K is the kinetic energy of the electron. This increase shifts the transition frequencies in the cyclotron Landau levels by an amount proportional to the cyclotron quantum number,

$$\Delta\omega_c' = -\delta(n + 1 + \frac{1}{2}s), \tag{4.6}$$

where

$$\delta = \omega_c(\hbar\omega_c/mc^2). \tag{4.7}$$

This is illustrated in Fig. 4.1. For $\omega_c/2\pi$ =147.7 GHz we have $\delta/2\pi$ =177 Hz so that $\delta/\omega_c' = 10^{-9}$. As can be seen from the energy level figure, the spin up n=0 state is nearly degenerate with the spin down n=1 state. This is a consequence of the fact that the g factor for the electron is nearly 2. As discussed in Chapter 1, the crucial measurements for determining the electron g factor are that of the cyclotron frequency, ω_c, and the spin flip frequency, ω_s. However, the g factor can be deduced

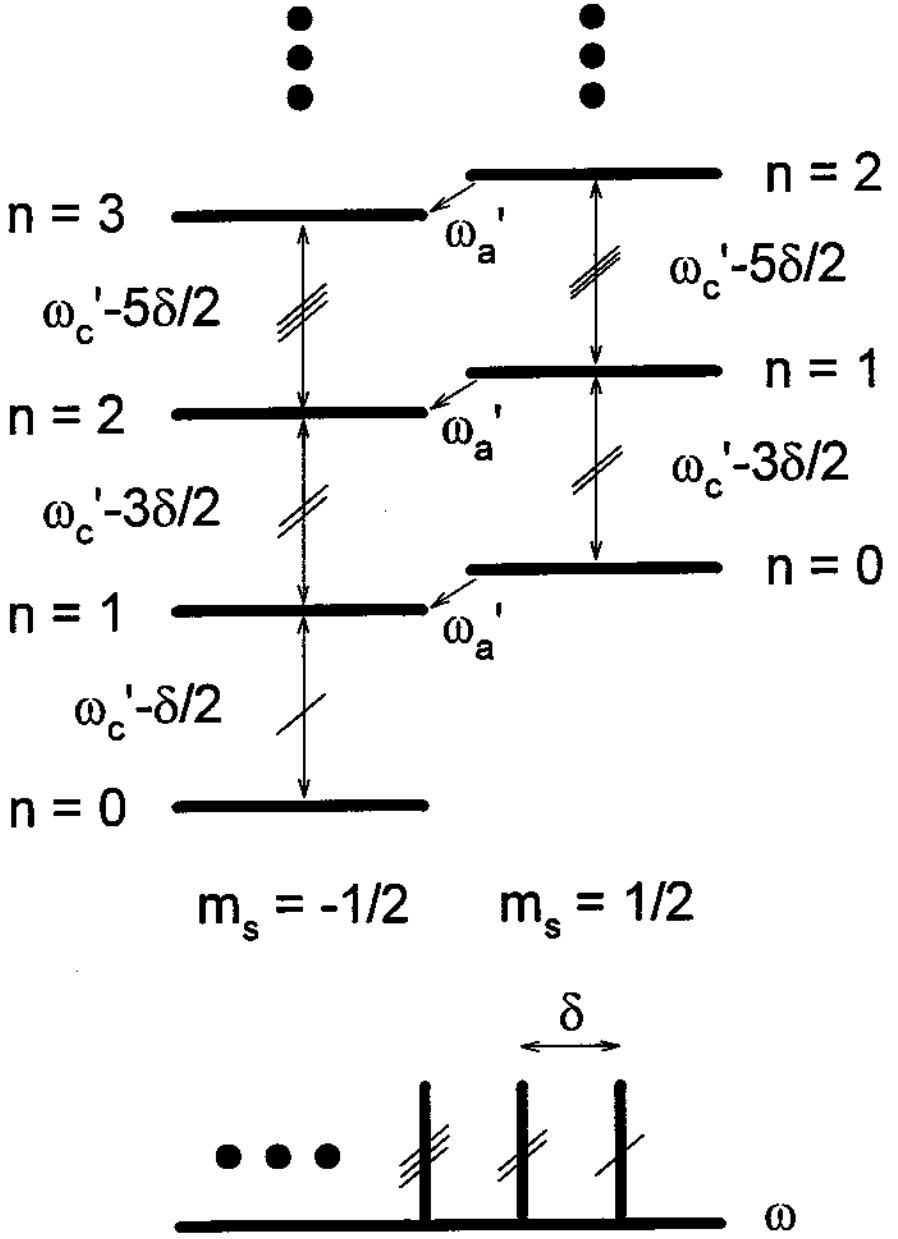

Figure 4.1: Landau ladders for the electron spin-cyclotron motion. The levels are shifted by relativistic corrections. The transition frequencies are spaced apart by δ, which is approximately one billionth of the cyclotron frequency.

from a measurement of the anomaly frequency, $\omega_a = \omega_s - \omega_c$. This is a simultaneous spin flip and cyclotron transition. This permits a difference measurement of two large frequencies, thereby increasing the precision [22].

Among these Landau levels, the electron probability is spread according to the Boltzmann thermal distribution,

$$P(n) = (1 - e^{-\hbar\omega_c/kT})e^{-n\hbar\omega_c/kT}, \tag{4.8}$$

which gives $P(0) = 82$ percent. Because of the relativistic coupling to the axial motion (as discussed in Chapter 2), the axial temperature produces a thermal width to each of these cyclotron levels, given approximately by,

$$\frac{\Delta\omega_c}{\omega_c} = -\frac{1}{2}\frac{\delta}{\omega_c}\frac{kT}{\hbar\omega_c}. \tag{4.9}$$

Similarly, an external magnetic bottle will also cause a broadening of the cyclotron line, as discussed in Chapter 2. The thermal width results from the total coupling from the relativistic coupling and the external magnetic bottle, as discussed in Chapter 2. The external magnetic bottle is measured in the hyperbolic trap to be -0.4 times the relativistic coupling. Since at 4.2 K $\hbar\omega_c/kT = 1.7$, the total coupling results in a thermal width of 0.18δ, where δ is the spacing between levels. This can be reduced either by reducing the axial thermal temperature, or by reducing the coupling between the axial and cyclotron oscillators (which also decreases the detection sensitivity). The external magnetic bottle used in the latest g factor determination [85] was 150 G/cm^2, which is about 30 times the relativistic bottle coupling size. This gives a thermal width of 9 δ. As discussed in Chapter 2, it is possible to adjust the external magnetic bottle coupling to cancel, partially or completely, the relativistic coupling [39]. External bottle sizes of 30 G/cm^2 and 10 G/cm^2 have been tried. (Recall that the relativistic bottle is about -5 G/cm^2.) Thus, the 10 G/cm^2 will cancel and reverse the overall bottle, giving +5 G/cm^2, with a thermal width of 0.3δ. A measurement of the cyclotron frequency should be attempted with the relativistic bottle almost completely cancelled, that is, where there is no thermal width [39].

Observed cyclotron excitations take the electron from the ground state (n=0) to an average energy of as large as 16.2 eV (n=26,500). This excitation is used to determine the unexcited cyclotron frequency. As described in the previous chapter, the cyclotron frequency was determined to a one δ precision, which is the precision needed to distinguish the spin state of the electron (see Fig. 4.1). In modelling the excitation, the natural question arises of how to describe both the high energy and the low energy regimes. Is the high energy excitation indeed a 'classical' state? What are the noise properties of the excitation process, and hence what are the requirements on the microwave source and magnetic field? We wish to discover a description for a damped, driven (time-dependent), anharmonic oscillator valid throughout the entire excitation range. We begin by looking at solvable cases such as the simple harmonic oscillator and the two state system as approximations to the electron system. Ultimately, the system can be described by a density matrix equation, known as the master equation; however, some information can be readily obtained using simpler models.

4.1 Preliminary Models

4.1.1 Two State Model

We review the properties of the two state system including Rabi flopping, adiabatic fast passage, and dressed states. The two state model will give an estimate of the drive field strength. The model can be used because the Landau levels are not harmonic, being slightly shifted due to special relativity. Therefore, we treat the n=0-1 transition, say, as isolated from the n=1-2 transition.

The transition probability for a drive swept through the resonance of a two-state system is given by the Landau-Zener formula [97],

$$P = 1 - e^{-2\pi\Gamma_{LZ}}, \tag{4.10}$$

where

$$\Gamma_{LZ} = {\Omega_{Rabi}}^2/4(d\omega_{drive}/dt) \tag{4.11}$$

is the Landau-Zener parameter. For slow sweeps, the population will follow an eigenstate of the combined 'atom' and field system (known as a 'dressed state'). This effectively transfers the population from the lower state (below resonance) to the upper state (above resonance). This is known as adiabatic fast passage.

The excitation process up the Landau ladder may be described as a series of two-state transitions. The ground state (n=0) and the first excited state (n=1) can be viewed as the first two-state system. Once the particle is excited to the first state (n=1), the first excited state (n=1) and the second excited state (n=2) are then considered as the two-state system. In this way, the cyclotron motion can be stepwise excited. This can be done adiabatically using a drive whose frequency is swept through the successive resonances. In this approximation, since the Rabi frequency for a transition from n to n+1 is equal to $\sqrt{n}$ times the Rabi frequency for the n=1 to n=1 transition, adiabatic fast passage with a drive of constant amplitude will transfer the population to the k^{th} level with a total probability,

$$P_k = \prod_{k=1}^{n}(1 - e^{-2k\pi\Gamma_{LZ}}), \tag{4.12}$$

if successive passages are taken to be completely sequential and independent. Here, Γ_{LZ} refers to the n=0 to n=1 transition. The calculated transition probability rapidly converges after four or five two-level transitions are shown in Fig. 4.2.

The measured sweep speed dependence shows that the probability of an excitation falls off for sweeps faster than 7,000 δ per second (see Fig. 4.3). Using the two-state model, we infer that the Rabi frequency for the n=0 to n=1 transition, $\Omega_{Rabi} \approx 2\delta$.

The largest cyclotron excitation observed was to n=26,500. This also can set a value for the Rabi frequency by equating the power loss at the maximum excitation to the power supplied by the microwave drive (saturation). We have

$$\pi n \gamma_c = \sqrt{n}\Omega_{0,1}. \tag{4.13}$$

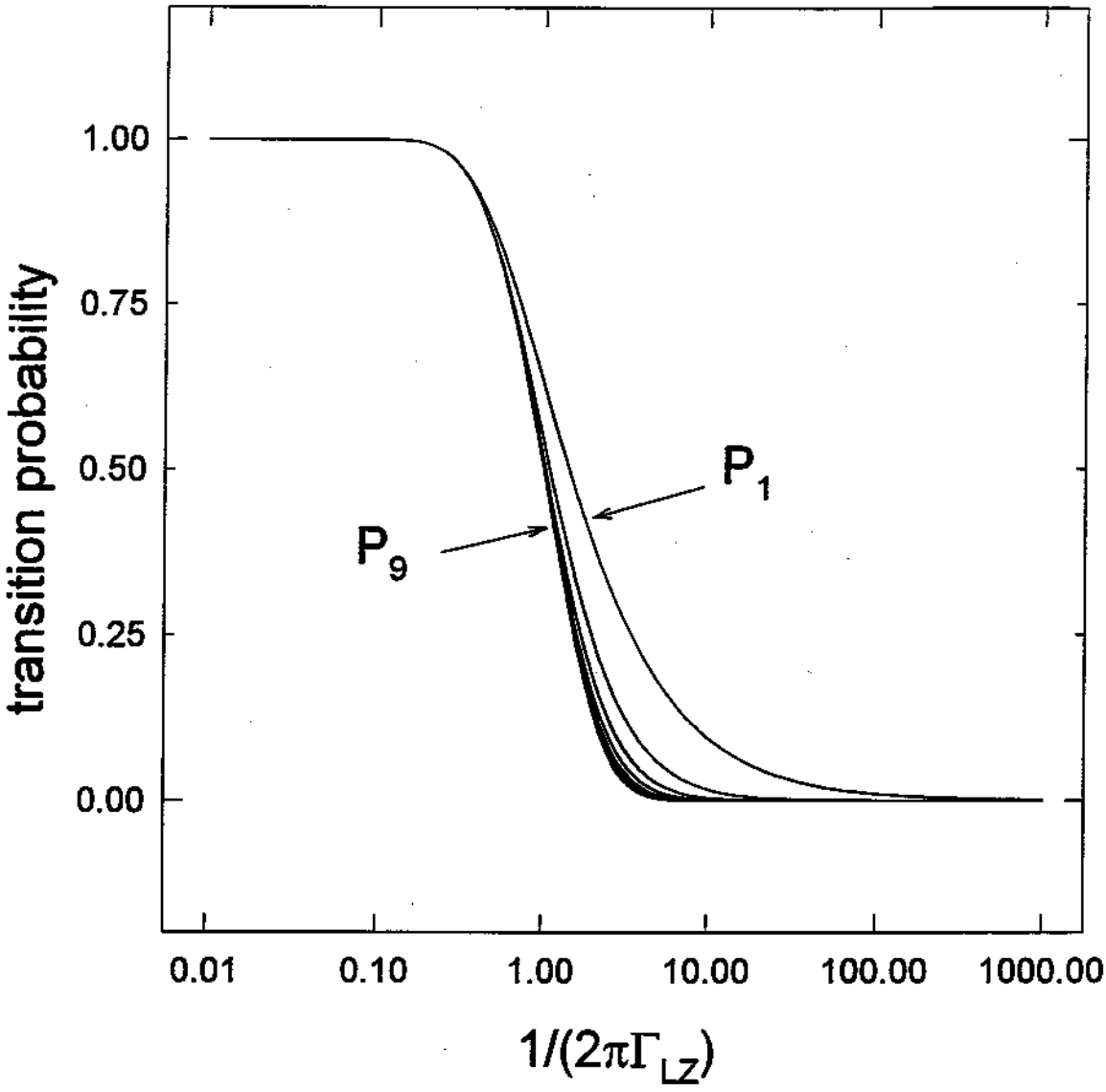

Figure 4.2: Calculated transition probability for a series of two-state excitations up the Landau ladder as a function of sweep speed. This rapidly converges after the first four or five two-state steps.

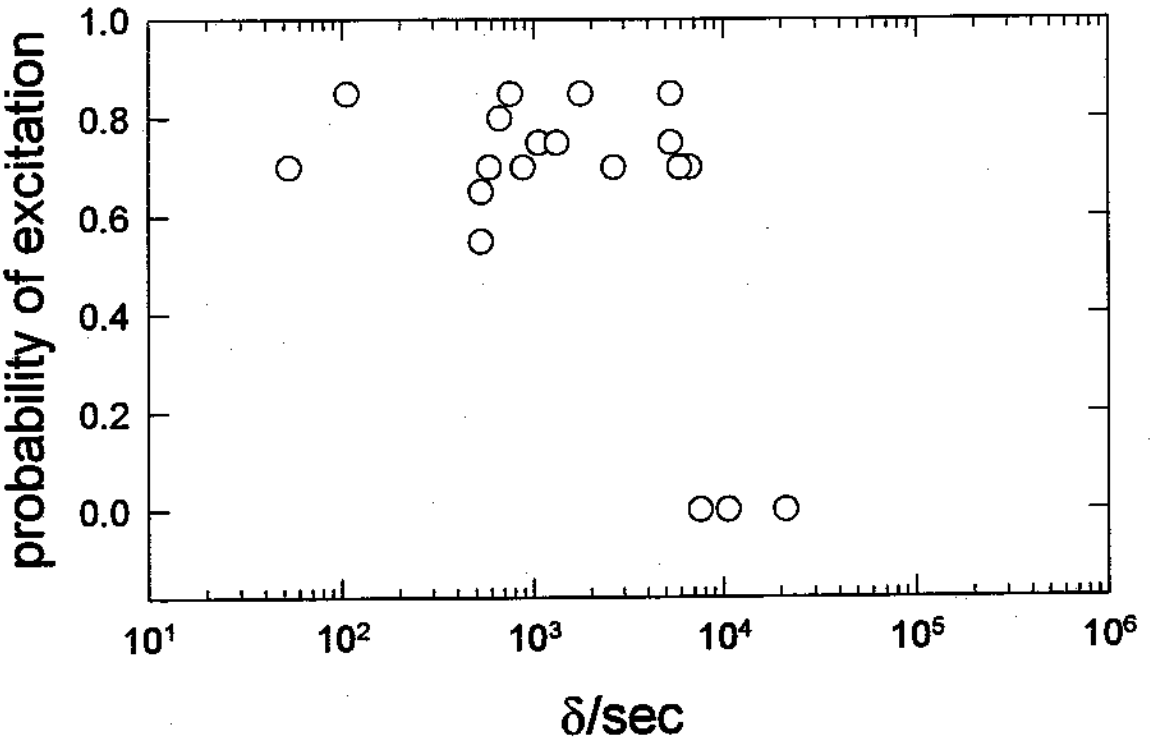

Figure 4.3: Sweep speed dependence of the probability of a cyclotron excitation falls off for sweep speeds faster than 7,000 δ/sec. This is slower than the response time limit of the magnet shim coils used to produce the excitation which is about 10,000 δ/sec.

This gives a Rabi frequency of 11δ. Because there may be other mechanisms for the excitation to collapse, this value is a lower limit on the Rabi frequency, and within an order of magnitude of the simple two-state model. The Rabi frequency gives the strength of the drive, which is of interest for possible cavity mode enhanced transitions that will be discussed later.

The Rabi frequency allows us to calculate the photon number density inside the trap volume. For harmonic oscillator number states interacting with a plane wave with an external field, E_0, through a dipole interaction, the Rabi frequency for the n to n+1 transition is

$$\Omega_{n,n+1} = qE_0\sqrt{\frac{n+1}{2m\hbar\omega}}. \tag{4.14}$$

The electric field strength can be related to the photon number density by

$$E_0^2 = (N/V)8\pi\hbar\omega, \tag{4.15}$$

giving

$$\Omega_{n,n+1}^2 = (N/V)\frac{8\pi q^2(n+1)}{2m}. \tag{4.16}$$

To saturate a transition, one half of the Rabi flopping period is equal to the decay time (the decay from the $(n+1)^{th}$ state is $(n+1)\gamma_c$),

$$\frac{T_{n,n+1}}{2} = \frac{1}{\gamma_c(n+1)} \tag{4.17}$$

or

$$\Omega_{n,n+1} = \pi\gamma_c(n+1). \tag{4.18}$$

The photon number density from the coherent drive required to saturate the transition is then

$$(N/V)_{saturated} = \frac{\pi\gamma_c^2 m(n+1)}{4q^2}. \tag{4.19}$$

For example, to saturate the n=0-1 transition requires 2×10^{-6}photons/cm^3. The incoherent 4.2 K blackbody radiation photon number density can be calculated by minimizing the free energy ($\partial F/\partial \mu = 0$) yielding

$$\frac{dN_\omega}{V} = \frac{1}{\pi^2 c^3} \frac{\omega^2 d\omega}{e^{\hbar\omega/kT} - 1} \tag{4.20}$$

which equals 1.7×10^{-8}photons/cm^3 for a bandwidth of γ_c about ω_c. Here, $\hbar\omega/kT = 1.7$. Thus, the photon number density required to saturate the n=0-1 transition is about 100 times the 4.2 K blackbody radiation density. The photon number density for $\Omega_R = 5\delta$, for example, is 10^{-2}photons/cm^3. This is 3×10^{-14}W, or -105 dBm. This low power, however, corresponds to many photons (1.3×10^7) per synchrotron decay time passing through the trap. For these estimates we assume that the Q of the surrounding cavity is approximately 1 in the hyperbolic trap. Thus, the photon loss rate from the cavity is fast, and the calculated transit time is valid. The time scales are summarized in Table 4.1.

If we represent the microwave drive as a collection of photons, then any absorbtion or emission will change the field seen by the electron. However, the number of photons passing through the trap during a synchrotron decay time is large. Therefore, we can still treat the microwave photons as a reservoir. If we treat the microwave drive as a classical external field plus a vacuum, which is equivalent to a quantum field in a coherent state, then the concept of photon number is not valid; nonetheless, the power estimates derived from the photon number density calculations are valid.

A treatment more general than the two state model involves the entire anharmonic oscillator energy level ladder. A straightforward integration of the many level Schröedinger equation yields the same characteristic transfer of population from the ground state to a high n state. Enroute to the final excitation, the population is widely distributed among the n levels, but regroups once the drive frequency becomes stationary. Incorporation of spontaneous emission decay in this model requires a Monte Carlo scheme [88, 32, 70]. Because the spontaneous emission photons

process	time scale [sec]
$2\pi\omega_c^{-1}$(at 147.7GHz)	7×10^{-12}
transit time (across 1 cm)	3×10^{-11}
time between photons	3×10^{-9}
$2\pi\Omega_R^{-1}$(at 5δ)	1×10^{-3}
$2\pi\delta^{-1}$(at 177Hz)	6×10^{-3}
γ_c^{-1}(at 3.7Hz)	4.3×10^{-2}

Table 4.1: Summary of time scales for cyclotron motion.

are not detected in the experiment, an ensemble average of the Monte Carlo simulations is needed to describe the experimental situation. Furthermore, the number of levels involved (up to 26,500) makes this simulation practically difficult. If one were able to describe the excitation in terms of coherent states, or in terms of dressed states, the time integration may be more tractable. It is also possible that the high excitations mimick the classical anharmonic oscillator behavior, which might make the computation easier. The master equation for the system is presented in a later section.

4.1.2 Coherent States

The simple harmonic oscillator with a forcing term and damping gives the familiar Lorentzian response. The angle θ is related to the detuning Δ by $\cot\theta = \Delta$. The detuning is in terms of half linewidths, $\Delta = [\omega - \omega_0]/(\gamma/2)$. See Fig. 4.4. This may be described quantum mechanically using coherent (Glauber) states [75, 46]. These are minimum uncertainty states, and are eigenstates of the destruction operator. The coherent states form minimum uncertainty wavepackets, and so mimick a classical particle trajectory. The ground state (n=0) is itself a coherent state. It can be shown that a harmonic oscillator initially in a coherent state, will evolve under the influence of an arbitrary external force to another coherent state with an eigenvalue for the destruction operator, a,

$$Z = e^{i\omega(t_2-t_1)} i \int_{t_1}^{t_2} dt \frac{f(t)}{\sqrt{2m\omega}} e^{i\omega(t-t_1)}. \tag{4.21}$$

To describe the effect of damping, density operator methods must be invoked. These will be discussed later. The density operator and coherent state description have the advantage of resembling a classical wavepacket. Unfortunately, incorporating the anharmonicity and the time-dependent drive complicate the description sufficiently to require numerical approaches.

The classical description of the anharmonic oscillator is discussed in [64]. The basic features are bistability and hysteresis. The response of a damped, driven anharmonic oscillator is shown in Fig. 4.4. The anharmonicity produces two stable branches (bistability) and an excitation that depends on the direction of the frequency sweep (hysteresis). Describing the anharmonic oscillator quantum mechanically with coherent states gives rise to the interesting features of quantum collapse and revival [94, 96]. Consider the anharmonic oscillator Hamiltonian,

$$H = \hbar\omega_0(a^\dagger a + \frac{1}{2}) - \frac{1}{2mc^2}(\hbar\omega_0(a^\dagger a + \frac{1}{2}))^2 \tag{4.22}$$

Since this is diagonal in the $|n>$ basis (only $a^\dagger a$ terms are involved in the Hamil-

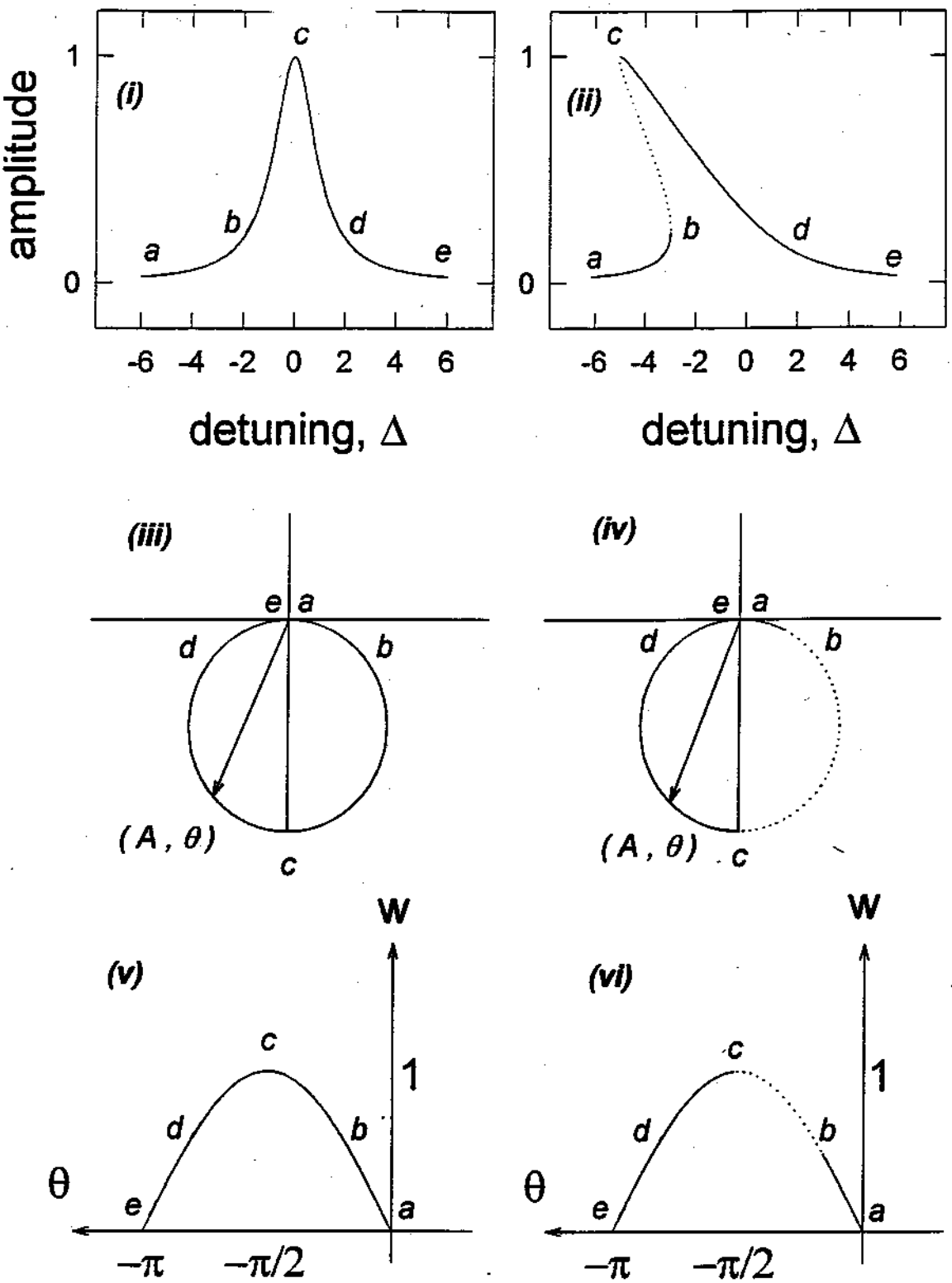

Figure 4.4: The response of a harmonic oscillator (left) compared to that of an anharmonic oscillator(right). Graphs (i, ii) are lineshapes; (iii,iv) phase space plots; and (v,vi) locus of attractors.

tonian), we can express the energy spread of a coherent state $|\alpha>$ as

$$\frac{\Delta H_\alpha}{<H>_\alpha} = \frac{\sqrt{<H^2>_\alpha - <H>_\alpha^2}}{<H>_\alpha} \approx \frac{1}{|\alpha|}\frac{1-2\beta|\alpha|^2}{1-\beta|\alpha|^2} \approx \frac{1}{|\alpha|}. \tag{4.23}$$

This is for large $|\alpha|^2$ and small β such that $\beta|\alpha|^2$ is small. (For the relativistic electron cyclotron oscillator, $\beta = \delta/2\omega_c$.) Therefore, the energy is well-defined. As is the case with the simple harmonic oscillator described by coherent states, the relative dispersion over N is small, but a large number of $|n>$ states are superimposed. In contrast, the wavepacket spread $<\Delta x_\alpha>^2$ deviates from the minimum uncertainty wavepacket of the simple harmonic oscillator with a repeating collapse and revival. The wavepacket spread relative to the minimum uncertainty spread of a simple harmonic oscillator coherent state is given by

$$\Delta \equiv \frac{(\Delta x)^2 - x_0^2}{x_0^2}\frac{1}{2N} \approx 1 - e^{2|\alpha_0|^2(cos\delta t - 1)}. \tag{4.24}$$

Here, $x_0 = \sqrt{\hbar/2m\omega}$ is the wavepacket spread of a simple harmonic oscillator coherent state. Δ will vary between 0, (corresponding to the minimum wavepacket spread), and 1. See Fig. 4.5. The period of recurrence is $2\pi/\delta$, the inverse of the anharmonicity frequency. The decay of the coherence responsible for the collapse and revival depends on the damping in the system. This will be discussed in more detail in the section on density matrix approaches.

4.2 Master Equation

In this section we describe a quantum theory of damping for the anharmonic oscillator [66, 17]. An alternative approach is the Langevin method. The system is described by a master equation, which is the equation of motion of the density operator[18]. This is then converted to a c-number equation in the coherent state basis [23]. The system evolution can then be described in terms of a true joint probability density known as the Q-function. In non-linear systems, the Q-function is natural to describe squeezing [23]. It may be possible to observe such squeezing

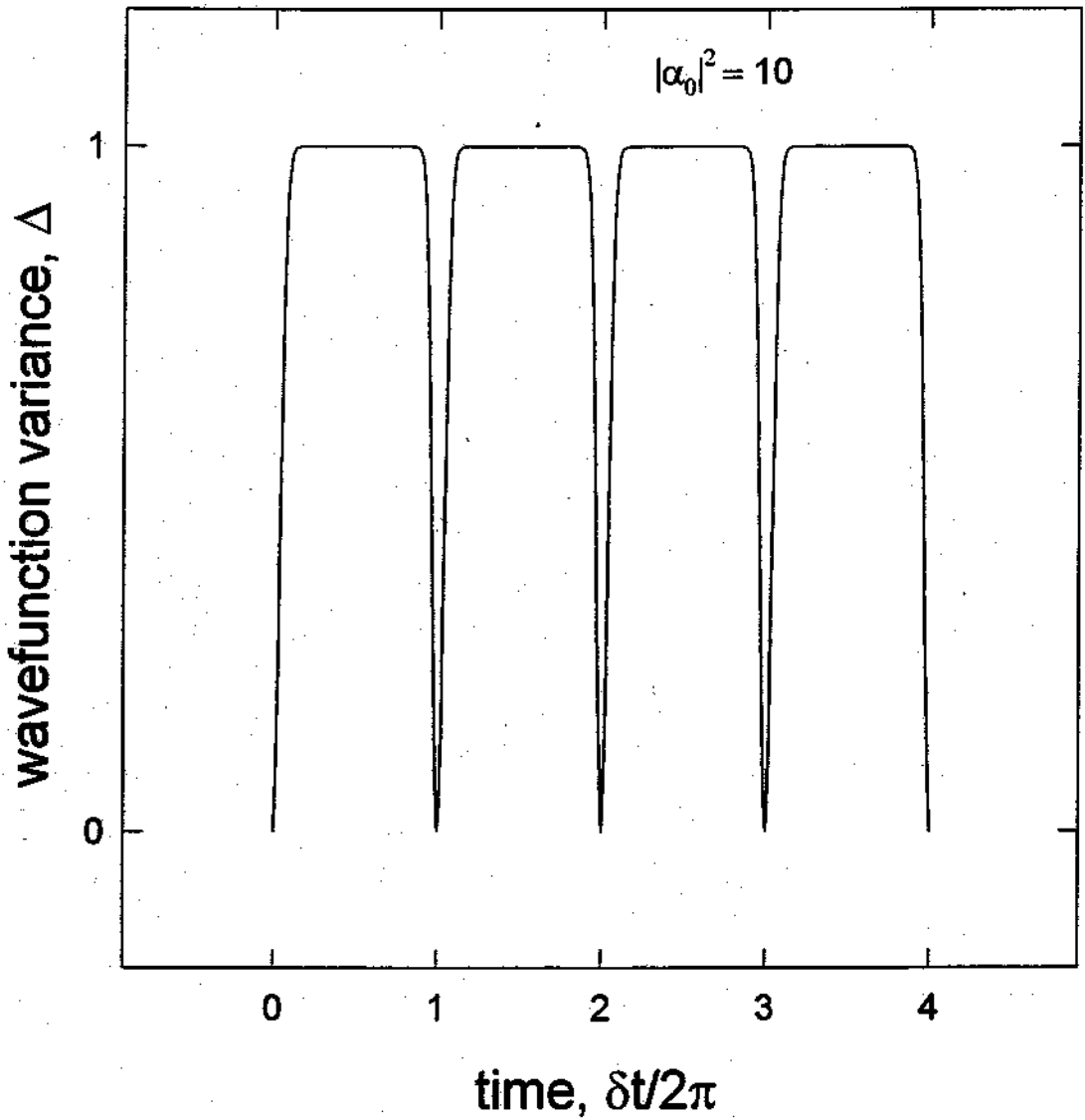

Figure 4.5: Calculated collapse and revival of the wavepacket spread of an anharmonic oscillator.

effects by parametrically driving the cyclotron motion of the electron. These master equation methods have been used to attempt to describe the transition between quantum mechanical and classical behavior. Quantum-coherence effects were found to be very sensitive to dissipation, and even the weakest damping was sufficient to restore classical behavior [16, 96, 67]. Furthermore, it has been noted that measurement is itself a form of dissipation [23, 16]. The Q-function equation for the damped, anharmonic oscillator can be analytically solved [23]. Unfortunately, the time-dependent drive case has not yet been solved.

The anharmonic oscillator system is shown in Fig. 4.6. The cyclotron motion of the electron at frequency ω_0, is slightly anharmonic (parameter μ) due to special relativity. This oscillator is, furthermore, coupled to (and broadened by) the axial motion of the electron at frequency, ω_z, and at temperature, T_z, through the relativistic bottle. The oscillator is damped through spontaneous emission by coupling to the modes of the cavity environment (quality factor Q). The cavity contains 4.2 K black-body radiation as well as coherent excitations due to an external microwave drive at frequency, ω_{drive}, and strength, Ω_{Rabi}.

Dissipation is treated by coupling the system to a reservoir of a collection of oscillators with a continuous distribution of frequencies [51]. Spontaneous emission is due to coupling of the system to the vacuum represented by the oscillator collection at zero temperature. Black-body radiation ($T \neq 0$) is incorporated by exciting the oscillators according to the Boltzmann distribution. See Fig. 4.7. In this way, excitation and decay processes in the system are accompanied by decay and excitation processes in the reservoir oscillators. The reservoir is assumed to have the property that it has no memory of the excitation; that is, the many degrees of freedom do not allow a coherent reexcitation of the system. This is the Markovian approximation. Because we wish to discover a simple description of the dissipative system, density operator methods are used whereby the details of the reservoir are summarized by tracing over the reservoir variables. Only the system variables are used. There are two time scales in this picture: a short time, τ_c, characterizing the fluctuations of the

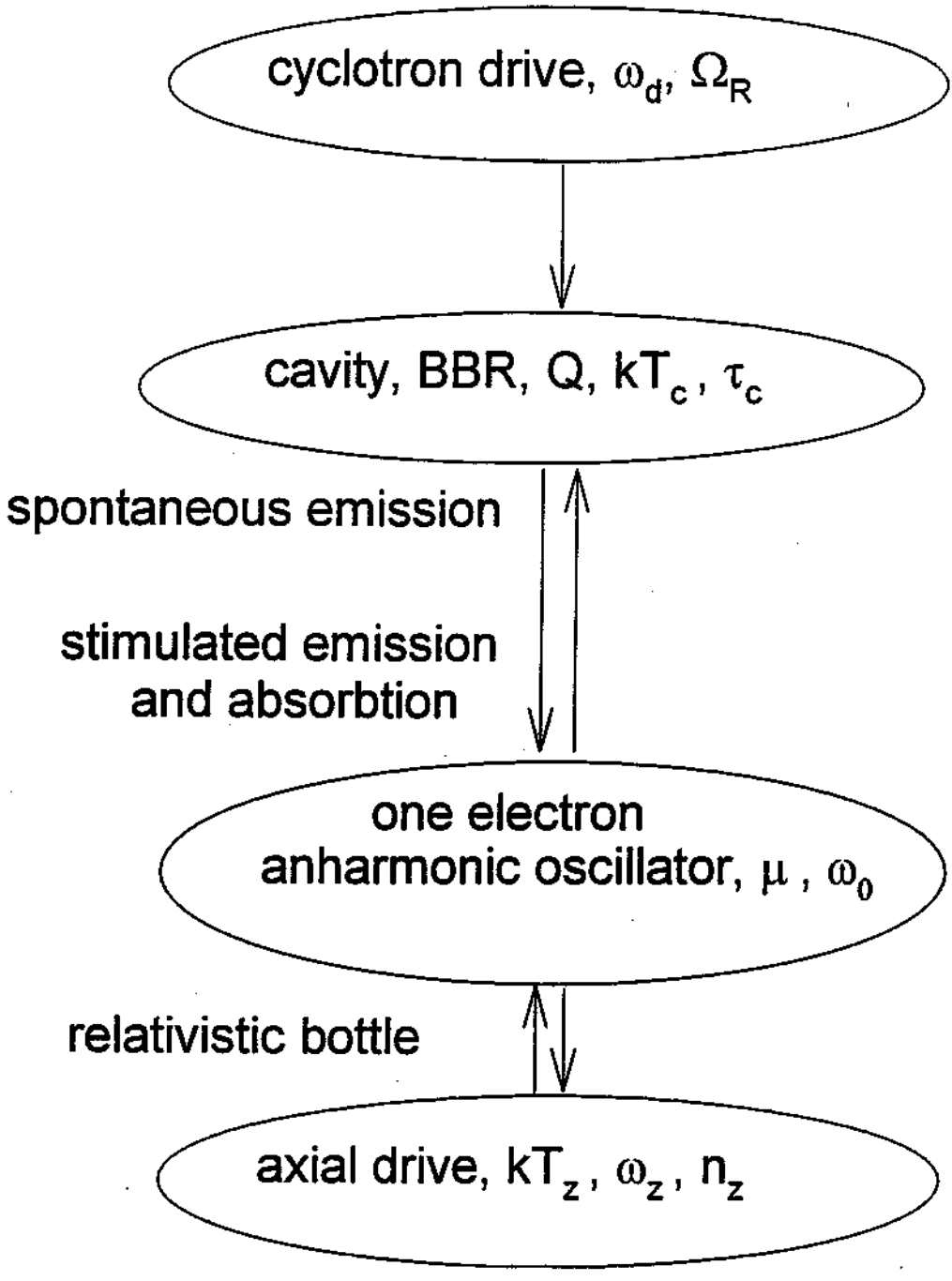

Figure 4.6: The electron cyclotron oscillator is thermally broadened by coupling to the axial oscillator. It is also damped by coupling to the cavity environment. An external drive excites modes in the cavity.

influence of the reservoir on the system, and a long time characterizing the kinetic evolution of the system. By considering a 'coarse-grained rate of variation', simple equations describing the evolution of the system can be obtained [20]. In analogy to Brownian motion, the evolution of the system also depends on the short time behavior of the fluctuations [33]. This is a consequence of the Fluctuation-Dissipation Theorem [17, 63].

The driven one electron relativistic anharmonic oscillator can be described by the Hamiltonian

$$\begin{aligned} H &= \hbar\omega_0(a^\dagger a + \frac{1}{2}) + \frac{\mu}{\hbar\omega_0}(\hbar\omega_0(a^\dagger a + \frac{1}{2}))^2 \\ &\quad +\hbar[a^\dagger \sum_j g_j b_j e^{-i\omega_j t} + a\sum_j g_j^* b_j^\dagger e^{i\omega_j t}] \\ &\quad +\hbar[v(t)a^\dagger + v^*(t)a]. \end{aligned} \tag{4.25}$$

The first line is diagonal in the number operator, and has the anharmonicity parameter $\mu = -\hbar\omega_0/2mc^2 \approx -1.2 \times 10^{-9}$. The second line describes the dipole coupling to the reservoir, which is our model for dissipation. The third line describes the coupling to an external drive. This can be converted to a reduced density operator equation, known as the master equation,

$$\begin{aligned} \frac{\partial\hat{\rho}}{\partial t} &= -i\mu\omega_0[(a^\dagger a)^2, \hat{\rho}] \\ &\quad +\frac{\gamma}{2}[2a\hat{\rho}a^\dagger - a^\dagger a\hat{\rho} - \hat{\rho}a^\dagger a] \\ &\quad +\gamma\bar{n}[a^\dagger\hat{\rho}a + a\hat{\rho}a^\dagger - a^\dagger a\hat{\rho} - \hat{\rho}aa^\dagger] \\ &\quad -iv(t)[a^\dagger, \hat{\rho}] - iv^*(t)[a, \hat{\rho}] \end{aligned} \tag{4.26}$$

where the interaction picture takes $H_0 = \hbar\omega_0(a^\dagger a + \frac{1}{2})$. Alternatively, we can take $H_0 = \hbar\omega_0(a^\dagger a + \frac{1}{2}) + \frac{\mu}{\hbar\omega_0}(\hbar\omega_0(a^\dagger a + \frac{1}{2}))^2$, which is still diagonal in the number operator. However, the first Hamiltonian has a solution in terms of coherent states.

Using the scaled damping and time, $\kappa = \gamma/2$ and $\tau = \omega t$, this is then changed into a Q-function equation,

$$\frac{\partial Q}{\partial\tau} = i\mu\alpha(1+2|\alpha|^2)\frac{\partial Q}{\partial\alpha} - i\mu\alpha^*(1+2|\alpha|^2)\frac{\partial Q}{\partial\alpha^*} + i\mu\alpha^2\frac{\partial^2 Q}{\partial\alpha^2} - i\mu\alpha^{*2}\frac{\partial^2 Q}{\partial\alpha^{*2}}$$

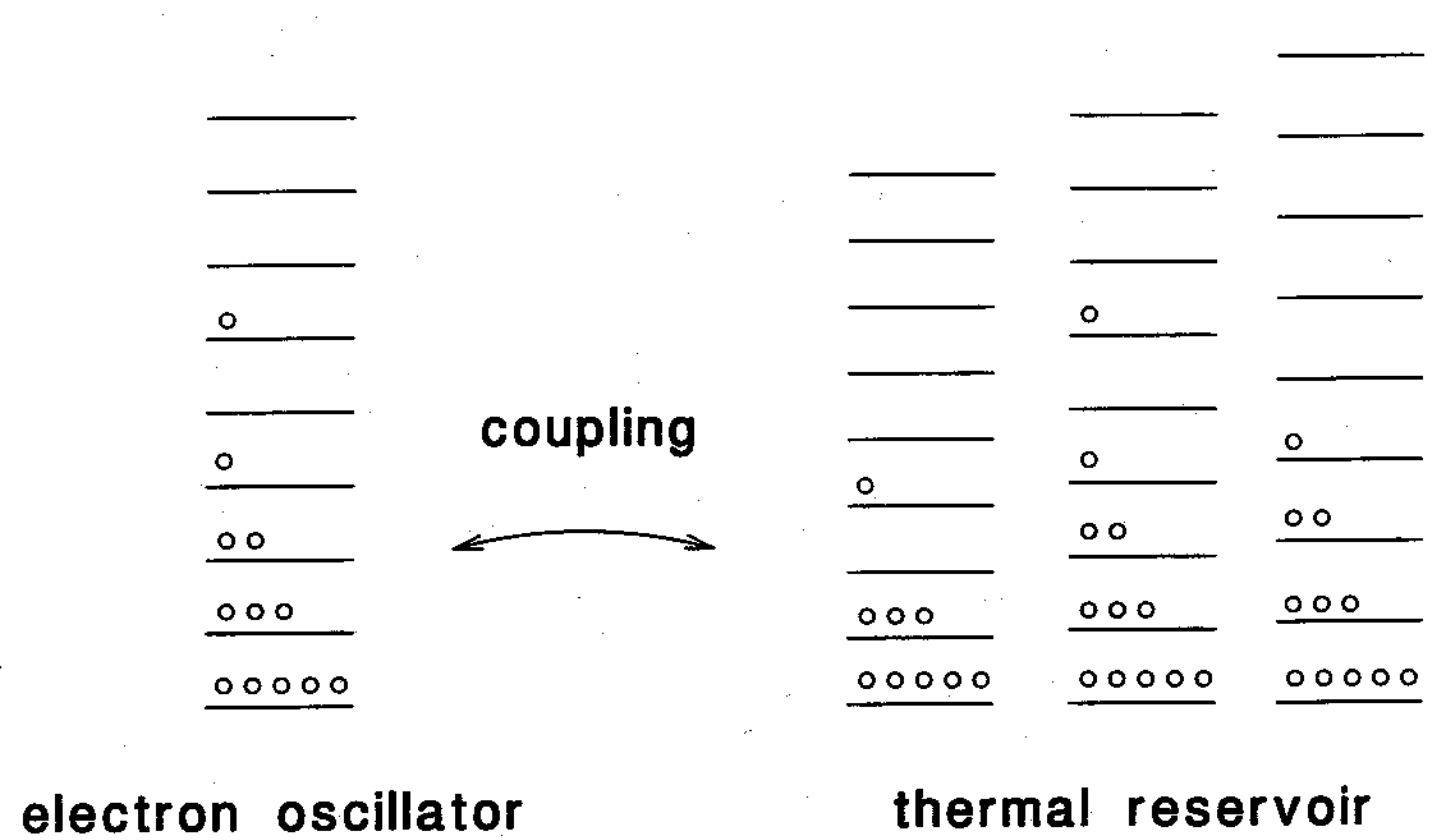

Figure 4.7: Spontaneous emission and black-body radiation are treated by coupling the system to an infinite series of oscillators that are excited according to the Boltzmann distribution.

$$+\frac{\kappa}{2}[\frac{\partial}{\partial\alpha}\alpha+\frac{\partial}{\partial\alpha^*}\alpha^*]Q+\kappa(\bar{n}+1)\frac{\partial^2 Q}{\partial\alpha\partial\alpha^*}$$
$$+i\frac{v(t)}{\omega_0}e^{i\omega_0 t}\frac{\partial Q}{\partial\alpha}-i\frac{v^*(t)}{\omega_0}e^{-i\omega_0 t}\frac{\partial Q}{\partial\alpha^*} \tag{4.27}$$

where $Q(\alpha,\alpha^*,t)=Tr(\rho(t)|\alpha><\alpha|)$. The Q-function is a probability density in phase space. The case without v(t) has been solved by Milburn [23]. The case with a drive, v(t), but without anharmonicity is presented by Louisell[66]. An analytical solution for the complete problem has not been found.

Numerically, this can be solved by projecting onto the energy basis, $|n>$[20]. Because the trace is representation independent, the particular choice of picture is not important except for ease of calculation. In the interaction picture, where $H_0=\hbar\omega_0(a^\dagger a+\frac{1}{2})+\frac{\mu}{\hbar\omega_0}(\hbar\omega_0(a^\dagger a+\frac{1}{2}))^2$, we have,

$$\begin{aligned}<k|\frac{\partial\tilde{\sigma}}{\partial t}|l> &= (\bar{n}+1)\gamma\sqrt{(k+1)(l+1)}\tilde{\sigma}_{k+1,l+1}\\ &+\bar{n}\gamma\sqrt{kl}\tilde{\sigma}_{k-1,l-1}-\bar{n}((k+l+1)+(k+l)/2)\gamma\tilde{\sigma}_{k,l}\\ &-iv(t)\sqrt{k}\tilde{\sigma}_{k-1,l}-\sqrt{l+1}\tilde{\sigma}_{k,l+1}\\ &+iv^*(t)\sqrt{k+1}\tilde{\sigma}_{k+1,l}-\sqrt{l}\tilde{\sigma}_{k,l-1}.\end{aligned} \tag{4.28}$$

This can be addressed numerically, though for large excitations, the matrix size becomes prohibitive. Treatment using the dressed states approach may be more effective in that the evolution of the density matrix will closely follow a basis vector, and thereby reduce the computational effort.

What are the approximations involved in this description? In order to treat the thermal radiation field and vacuum as a reservoir, or heat bath, the reservoir must depend only on the present and not on the past. There is no memory of the past. Therefore, any excitation from the electron system that is transferred into the reservoir will not return into the system. This is called the Markovian approximation, as discussed earlier. In other words, the correlation time of the reservoir, τ_c, must be fast compared to the system damping time, ${\gamma_c}^{-1}$, and to all other time scales involved in the system (${\omega_0}^{-1}, \delta^{-1}$). (See also the discussion of 'motional narrowing' in [20].) For example, Fermi's Golden Rule is a linear

approximation to the Rabi flopping equation. This is valid for short times, or for incoherent systems where the coherence time is short and so will only allow a linear approximation. The Rabi formula is valid in systems where the coherence time is long. Thus, the separation of time scales in the Markovian approximation allows us to treat the reservoir as a heat bath, and the driving field as a coherent process. In order to treat the effect of spontaneous emission separately from the effect of a simultaneous external driving field, the evolution time of the system determined by a Rabi rate, $\Omega_{Rabi}{}^{-1}$, must be slow compared to the spontaneous emission time which is given by the correlation time of the reservoir, τ_c. Therefore, we can neglect the effect of the Rabi evolution during the time of the spontaneous decay. Furthermore, we must restrict the parameters so that we can treat the irreversible terms in the master equation as being unaffected by the non-linearity of the system. We require the damping to be weak, $\kappa << \omega_0$, and the non-linearity to be weak, $\mu << 1$. Also, the temperature is such that $\kappa << kT/\hbar < \omega_0$ so that $\bar{n}$, the number of thermal photons, is about zero. The thermal fluctuations in the reservoir, which decay with a time constant $\hbar/kT$, must be faster than the decay time of the system, γ^{-1}. These conditions are discussed in [50].

To illustrate, the above methods and considerations are applied to a damped, driven, simple harmonic oscillator at a temperature, T [66]. The conditional probability of finding the oscillator in a state characterized by β, β^* at time t is

$$p(\beta,\beta^*,t;\beta',\beta^{*\prime},0) = \frac{1}{\pi\bar{n}(1-e^{-\gamma t})} exp \frac{-|\beta-\beta' e^{-\gamma t/2}+w(t)e^{i\omega t}|^2}{\bar{n}(1-e^{-\gamma t})} \quad (4.29)$$

where $\beta = \beta' e^{-\gamma t} - w(t)e^{i\omega t}$ and variance $\zeta(t) = \bar{n}(1-e^{-\gamma t})$. This is a delta function at t=0, but then spreads out to a gaussian whose center of gravity decays at a rate γ, and is driven by $w(t)$. The spread is described by the variance, ζ. This has a limit dependent on the temperature of the damping reservoir, but the approach to this limit is characterized by γ. It is remarkable to note that a system initially in a coherent state will decay due to spontaneous emission to another coherent state.

From the master equation, we expect a similar result for the damped, driven, anharmonic oscillator at non-zero temperature. The probability distribution should resemble that of a classical particle which is broadened by a temperature. In addition, the non-linear terms will create collapse and revival structures due to quantum coherence, as discussed above. The time scale for collapse of coherence is discussed in [67]. The 'fringes' in the probability distribution (representing interference effects) will decay on a time scale $t = 1/\gamma|\alpha|^2$, which is much shorter than the 'contractive dynamics' time scale, $1/\gamma$, for large excitations ($|\alpha|^2$). Thus, for the experimental case of a highly excited, weakly damped ($Q = 10^{10}$), and slightly anharmonic oscillator the probability distribution, $Q(\alpha, \alpha^*, \tau)$ will quickly smear out into a ring in phase space. This is similar to the behavior calculated for a classical anharmonic oscillator [23]. Furthermore, the basins of stability around the attractors form a whorl in phase space. Around the attractor, the basin of attraction is almost a circular arc of thin radial extent. This has the implication that amplitude noise may be more important than phase noise in the microwave drive. Also, phase noise will be less important at higher excitations ($|\alpha|^2$).

4.3 Experimental Observations

Several characterizations have been made on the cyclotron excitation. Fig. 4.8 shows the bistability and hysteresis in an excitation of the cyclotron oscillator [39]. A large excitation is created when the drive is swept down in frequency; and little or no excitation is created when the drive is swept up in frequency. Fig. 4.9 shows an excitation of 10 eV, or n = 16,000. This was obtained by sweeping the magnetic field instead of the drive. In the figure, after about n=16,000, the axial frequency lock loop circuit drops out. Excitations of 16.2 eV (n = 26,500) have been observed. The behavior for the maximum excitation versus the microwave drive power is expected to be linear in the drive power ($\Omega_{Rabi} \sim n$) from Eq. 4.13; however, a quadratic dependence was found ($\Omega_{Rabi} \sim n^2$) (similar to superradiance [2]). See Fig. 4.10.

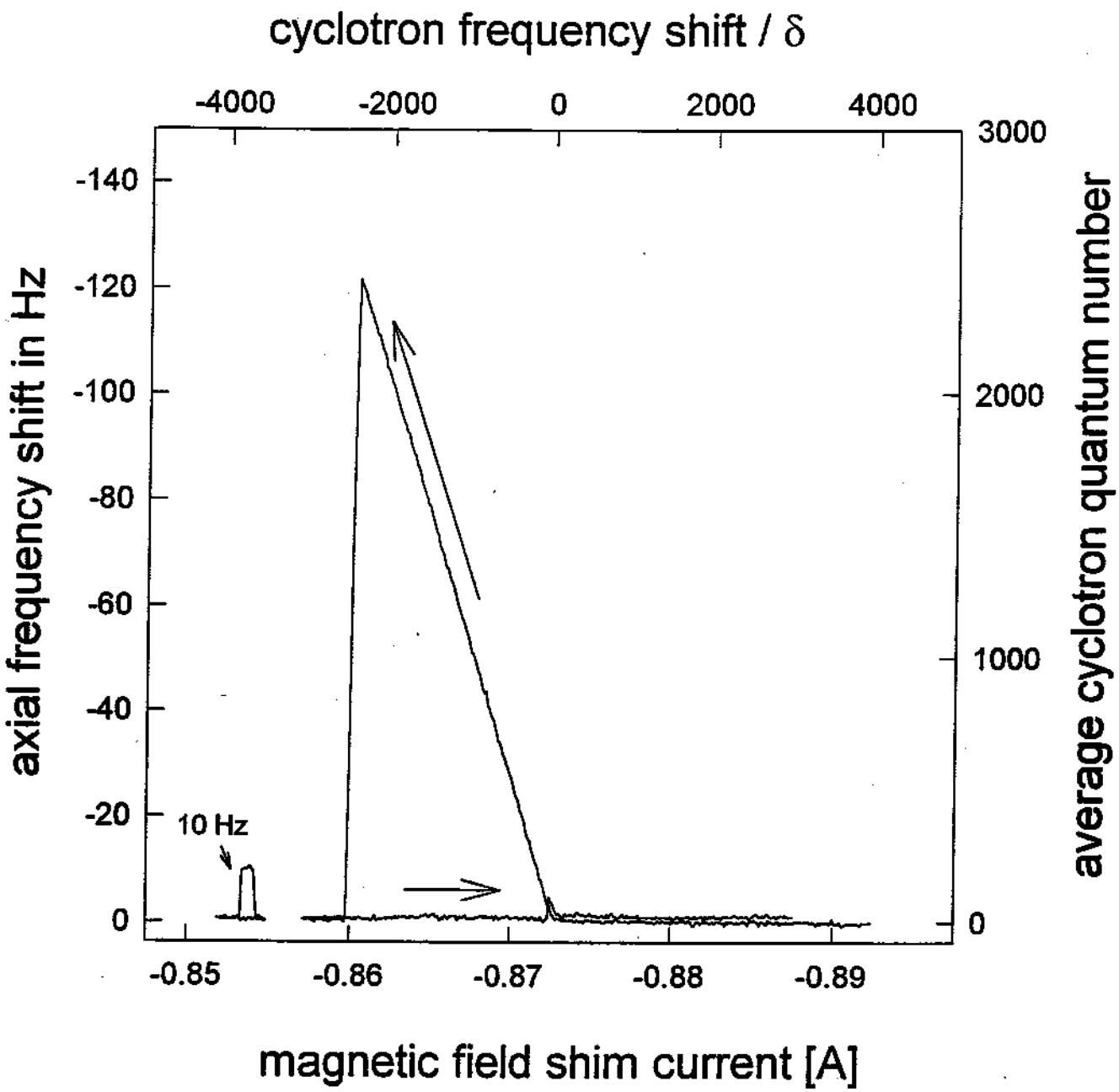

Figure 4.8: Relativistic, anharmonic cyclotron oscillator excitation showing bistability and hysteresis. Feature at left calibrates the axial frequency shift detector.

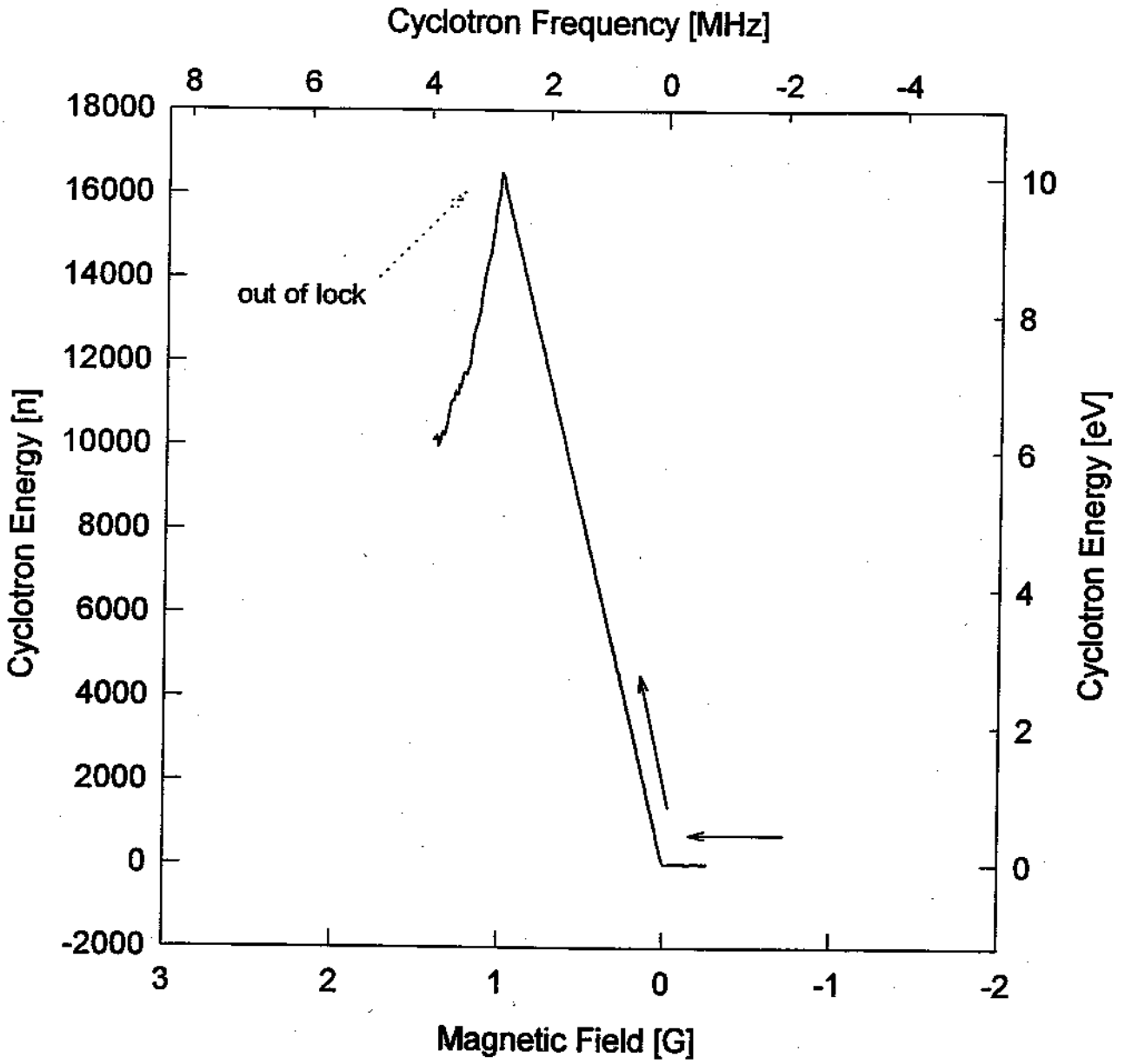

Figure 4.9: Large cyclotron excitation (10 eV) observed as the magnetic field is increased. Excitations as large as 16.2 eV (n=26,500) have been observed. After about n=16,000, the axial frequency loop goes out of lock.

process	value
cyclotron frequency, ω_0/ω_0	1
anharmonicity, $\mu = -\hbar\omega_0/2mc^2$	-6×10^{-10}
damping, $\kappa = \gamma_c/\omega_0$	2.5×10^{-11}
Rabi frequency, Ω_{Rabi}/ω_0	6×10^{-9}
coherence time, $\omega_0/\gamma_c\|\alpha\|^2$	1.5×10^6
temperature, $(kT/\hbar\omega_0)$	0.59
thermal occupation number, $\bar{n} = \frac{1}{e^{\hbar\omega_0/kT}-1}$	.22
correlation time of reservoir, τ_c	0

Table 4.2: Summary of time scales for master equation in the Markovian approximation.

This suggests that the mechanism responsible for the de-excitation of the cyclotron motion is not a simple competition between Rabi excitation and damping, but perhaps may be due to noise excitation or deexcitation processes. This re-enforces the earlier statement that the Rabi frequency estimate from the maximum excitation is a lower bound. Another characterization of the cyclotron excitation is the dwell rate (see Fig. 4.11). The oscillator is excited to a chosen energy, and the time it remains

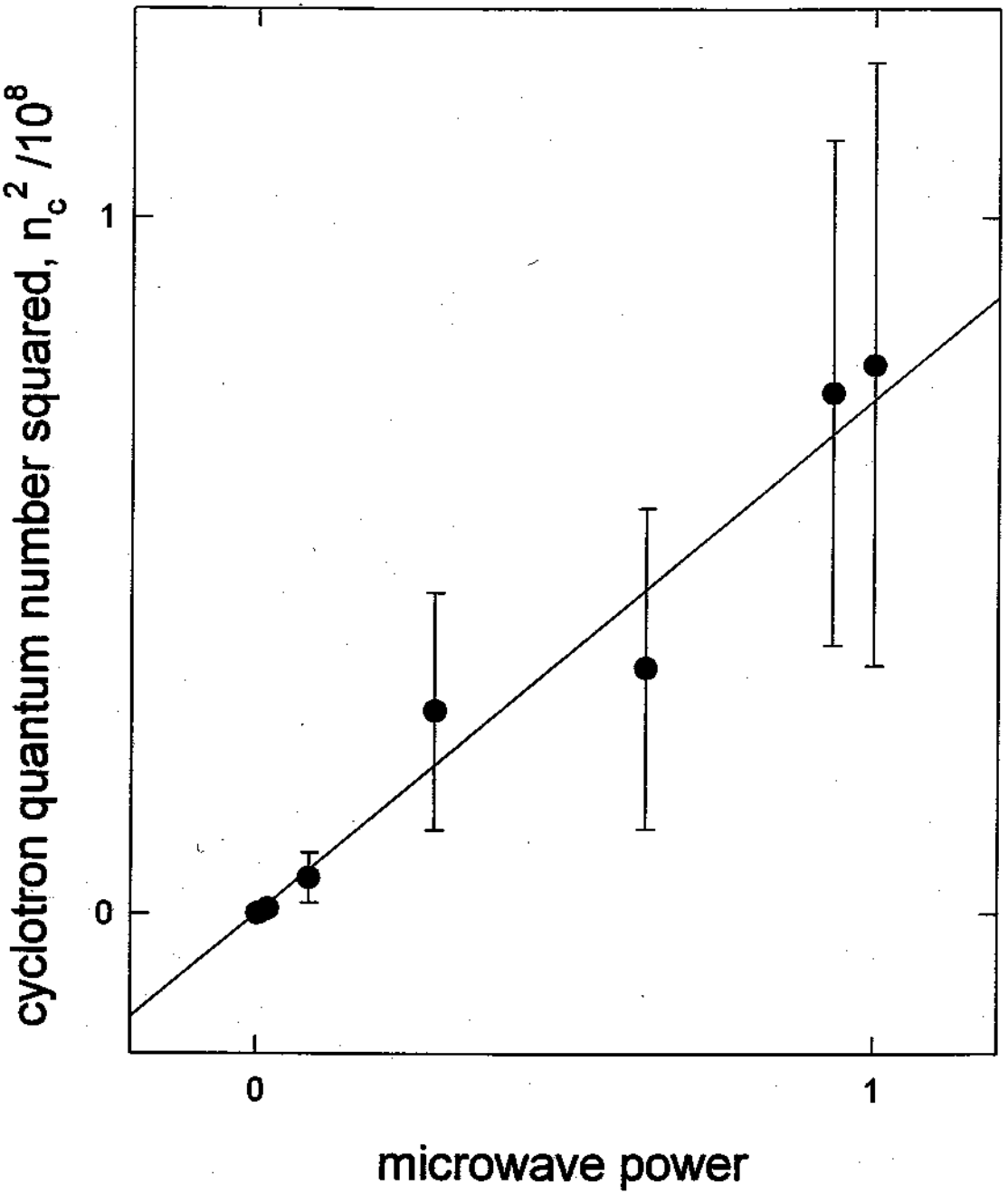

Figure 4.10: Maximum excitation of cyclotron oscillator versus microwave power. The expected behavior is linear in n; the measured behavior varies as n^2.

excited (with the drive still on) gives the dwell time. This presumably measures the noise excitation out of the stable 'bucket' around the attractor. This effect seems to be important for lower microwave power, and unimportant for high powers. The larger Rabi frequency probably compensates for noise deexcitation. It is also observed experimentally that sideband cooling of the magnetron motion makes it more likely to excite to high cyclotron energies.

4.3.1 Cavity Modes

The cyclotron oscillator interacts with the cavity modes in the Penning trap to modify the spontaneous emission rate [38, 83]. The modes have been studied extensively in the cylindrical geometry trap [76, 12, 13, 45]. The modes can be calculated analytically and identified with the signals measured by parametric excitation. This allows extreme control of the radiation environment of the electron, which is desirable for precision measurements. We measure one such mode with a cloud of electrons in the cylindrical trap by sweeping the magnetic field using a fine resolution (non-superconducting) magnetic field coil (see Fig. 4.12). This permitted the resolution of the splitting of the triplet peaks of a TE_{127} mode (evidenced by the double peaks at each triplet peak). The triplet is formed by the motional sidebands for an odd p mode (an even p will cause a doublet). These peaks would be degenerate were it not for slight geometric asymmetries in the trap electrodes due to cuts and slits or misalignments and deformations. This resolution demonstrates the precise control of the damping environment.

This control might be used to sideband cool the axial motion of a particle in a Penning trap [37]. A mode with the appropriate symmetry (p even, m = 1) will couple the axial and cyclotron motions to allow the extraction of energy from the axial motion and placement of energy into the cyclotron energy. Coupling the electron to a p odd mode will then damp the energy in the cyclotron motion. The

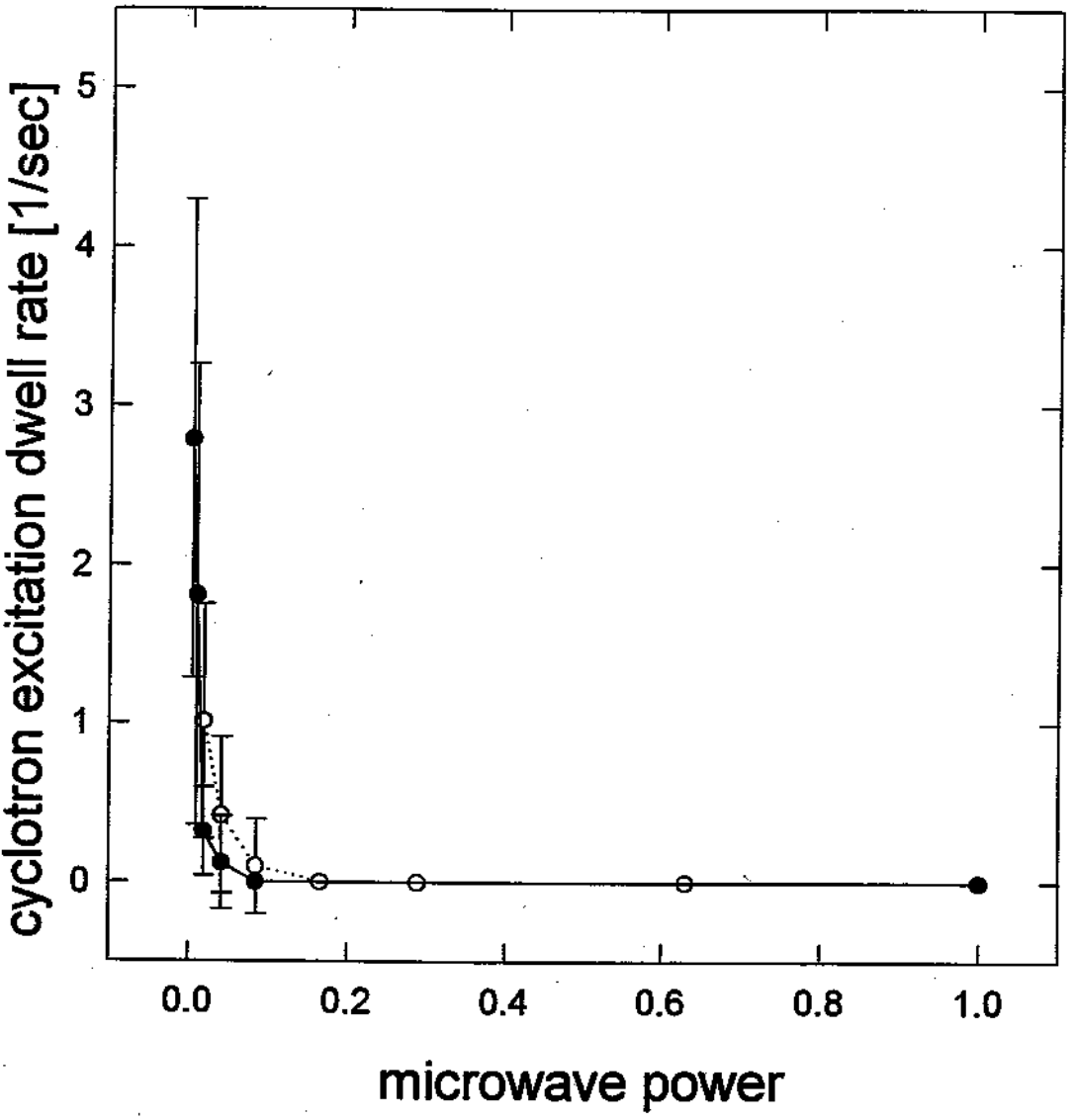

Figure 4.11: The dwell rate for 3 Hz (black) and 20 Hz (white) axial shifted cyclotron excitations versus microwave power. The excitation quickly dies for lower microwave powers, but remains for more than 3 hours for larger powers.

theoretical cooling limit is

$$T_z = \frac{\nu_z}{\nu_c'} T_c \tag{4.30}$$

which is about 2 mK for the frequencies considered here ($T_c = 4.2$K). To remain at this low temperature, the axial motion will have to be decoupled from the damping circuit, which would otherwise heat the motion back up to 4.2 K.

Coupling the axial and cyclotron motions through Lorentz forces require at the center of the trap that the axial force, $f_z \sim x$, and the transverse force, $f_x \sim z$. This implies that m=1 and p even. For TM modes, we have for the cooling rate on resonance for a weak drive

$$\frac{\gamma_0}{\gamma_c} = Q \left(\frac{E_0 d}{V_0}\right)^2 \left(\frac{p\pi d}{4z_0}\right)^2 \frac{{\omega_z}^3}{4{\gamma_c}^2 \omega_c} \left(\frac{\omega_c \omega_d}{\gamma_{1n}^2 c^2} - 1\right) \tag{4.31}$$

where $x_{mn} = \gamma_{1n}\rho_0$ is the n^{th} root of $J_1(x)$. Candidate modes near the present cyclotron mode, TM_{127}, are TM_{136} at 158.10 GHz, TM_{144} at 159.64 GHz, and TM_{142} at 144.64 GHz. The electric field $\sqrt{Q}E_0$ is enhanced by the Q-factor of a cavity mode. For a given microwave source power, the cooling rate also depends on a spatial volume average for the particular mode which is not included in Eq. 4.31. Estimating the electric field strength from the Rabi frequency approximated above, and taking a typical Q-factor for the modes of 1000, and a cyclotron damping time corresponding to the free space value, we estimate that $\gamma_0/\gamma_c \approx 1$, that is, the process will be saturated. Thus, the sideband cavity cooling looks like a promising way to cool the axial motion of the particle.

4.3.2 Two Particles

The cyclotron resonances for two particles in a Penning trap have been observed for the proton-proton, the antiproton-antiproton, the antiproton-H^- [41, 43], and, here, the electron-electron system. The cyclotron resonances for the heavier particles are weakly damped, a characteristic which allows a good fit to the exponential decay of the cyclotron excitation to obtain a precise measurement of the unexcited cyclotron

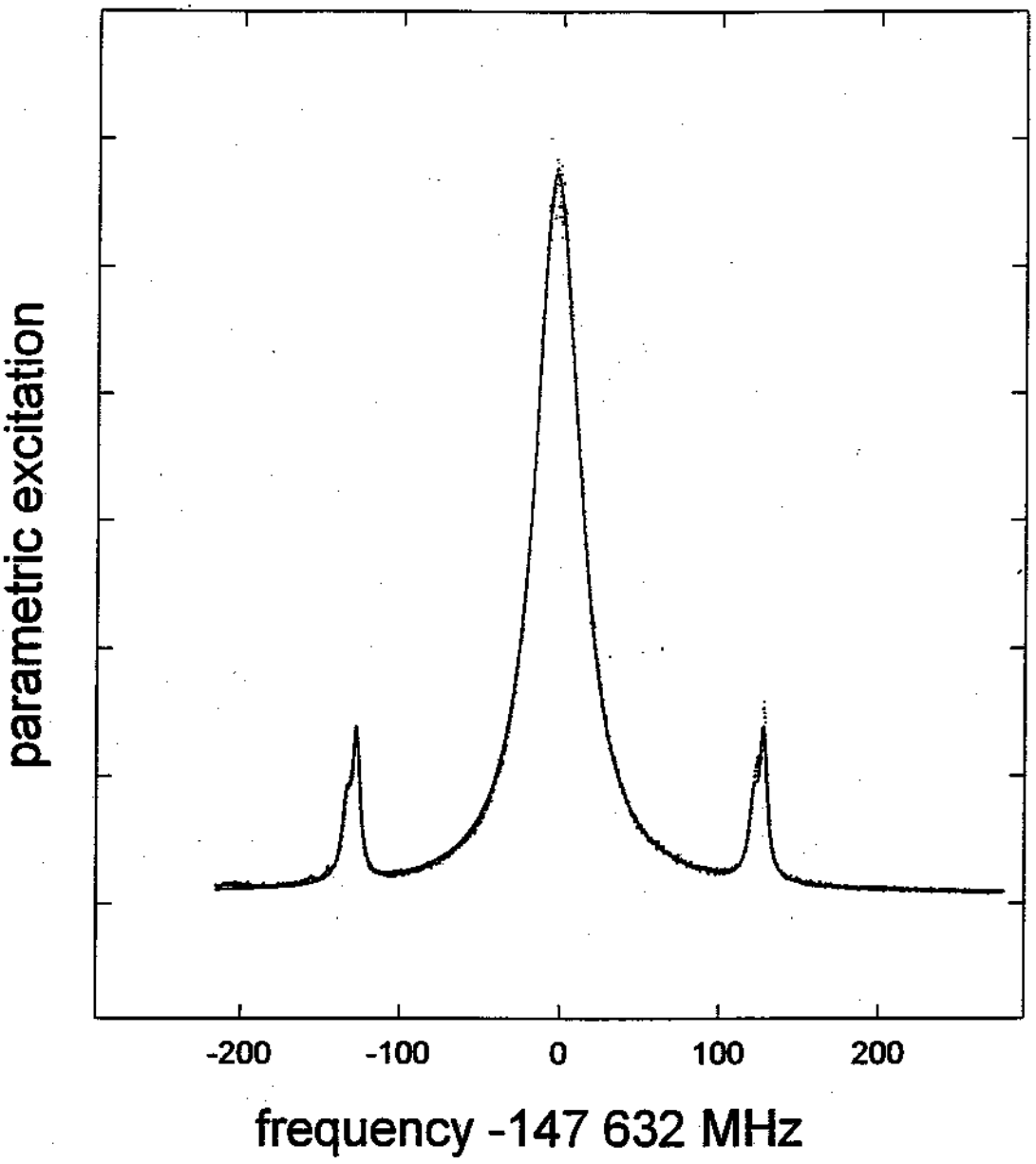

Figure 4.12: Microwave cavity mode showing splitting of degeneracy. The lineshape is constrained to fit to two triplet Lorentzians.

frequency. This has been used to measure [43] the ratio of the charge to mass ratios of the antiproton and proton as 1.000 000 000 5 ±0.000 000 001 1 . The resonance for two particles in a trap at the same time reveal a structure of frequency locking similar to nonlinear bifurcations. The initial cyclotron excitations are at different frequencies, but as they decay, they abruptly lock to a single frequency. The electron-electron system, on the other hand, is strongly damped by synchrotron radiation.

The observed resonance for two electrons is shown in Fig. 4.13 . The two particle signal is overlaid on the one electron resonance. The slope of the initial branch is $\eta_1 = 1.48$ (which is the same as for one electron), whereas the slope of the second branch is $\eta_2 = 2.41$. Here, $\eta \equiv \frac{\Delta\nu_c/\nu_c}{\Delta\nu_z/\nu_z}$. This can also be written as

$$\eta = \frac{2}{1 + (2c^2/\omega_z^2)(B_2/B)}, \tag{4.32}$$

which gives a value for the external magnetic bottle, $B_2/B = +3.1 \times 10^{-5}/\text{cm}^2$. If there were no external bottle, then $\eta = 2$, and $B_2/B = 0$ in the formula for η. The equivalent relativistic bottle is of strength $B_2/B = -8.9 \times 10^{-5}/\text{cm}^2$ at 5.3 Tesla. (See Chapter 2.)

The basic features of the two electron resonance can be explained by a simple model of two oscillators coupled by Coulomb repulsion. First, we estimate the relevant physical parameters. By setting the Coulomb repulsion equal to the trap energy, we obtain an equilibrium axial separation of $z_{eq} = 2 \times 10^{-3}$cm. The typical resonantly driven amplitude (extracted from the parametric resonance studies) is $z_d = 3 \times 10^{-2}$cm. The 4.2 K thermal motion is $z_{th} = 3 \times 10^{-3}$cm. The unexcited cyclotron motion has a radius of $r_c^0 = 1 \times 10^{-6}$cm. The excited radius scales as the square root of the excitation energy. We assume that the magnetron motion is cooled to the limit $r_{mag} = 6 \times 10^{-5}$cm. From these parameter estimates we assume the motion of the particles to be along the z axis, but perhaps separated in the x-y plane by a distance a. The equations of motion are then

$$m_1\ddot{z_1} = -kz_1 + \frac{q^2(z_1 - z_2 + a)}{|z_1 - z_2 + a|^3} - \gamma_z\dot{z_1}$$

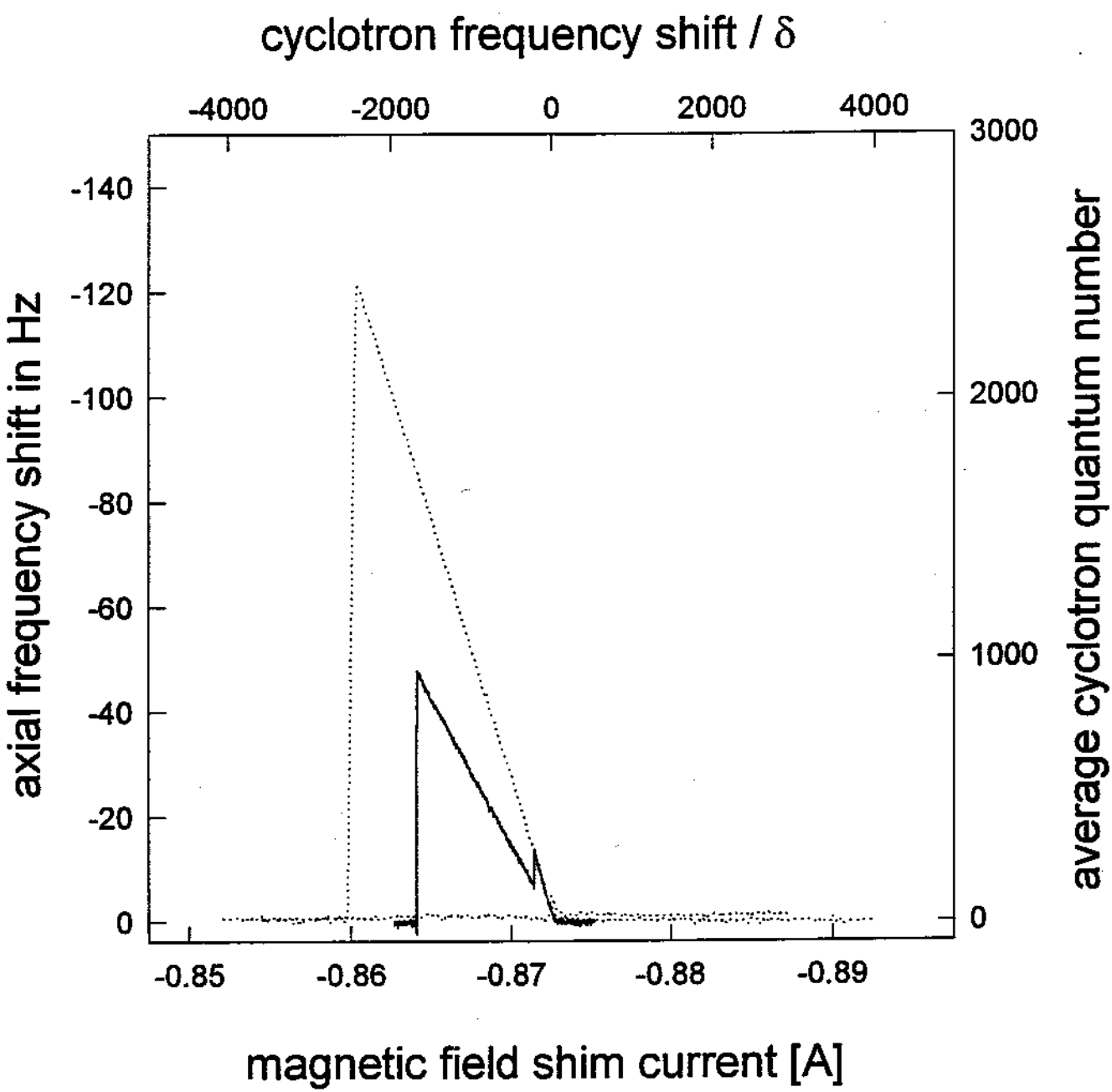

Figure 4.13: Observed cyclotron resonance for two electrons in Penning trap. The two particle signal is overlaid on the one particle signal.

$$m_2\ddot{z}_2 = -kz_2 - \frac{q^2(z_1 - z_2 + a)}{|z_1 - z_2 + a|^3} - \gamma_z\dot{z}_2 \tag{4.33}$$

where z_1, z_2 are the displacements from equilibrium. We add and subtract the equations to get the behavior of the normal mode motions, a center of mass motion and a breathing motion,

$$\begin{pmatrix} \tilde{z}_+ \\ \tilde{z}_- \end{pmatrix} = \frac{1}{2}\begin{pmatrix} z_1 + z_2 \\ z_1 - z_2 \end{pmatrix}. \tag{4.34}$$

The center of charge rather than the center of mass is actually detected. However, since $\gamma \approx 1$, these are about the same. We take $m_1 \approx m_2$. The equation of motion for the center of charge mode is then,

$$m\frac{\ddot{z}_1 + \ddot{z}_2}{2} = -k\frac{z_1 + z_2}{2} - 2\gamma_z\frac{\dot{z}_1 + \dot{z}_2}{2}. \tag{4.35}$$

Thus, the signal due to the center of charge is the familiar Lorentzian at a frequency

$$\tilde{\omega}_{z,+} = \sqrt{k/\frac{(m_1 + m_2)}{2}}. \tag{4.36}$$

Consider the case where the cyclotron motion of both electrons are excited. Then $m_1 = m_2 = \gamma m_0$, and

$$\tilde{\omega}_{z,+} = \sqrt{k/\gamma m_0}. \tag{4.37}$$

The variation in the axial frequency with respect to γ is $\frac{\Delta\tilde{\omega}_{z,+}}{\tilde{\omega}_{z,+}} = -\frac{1}{2}\frac{\Delta\gamma}{\gamma}$. The variation of the cyclotron frequency remains $\frac{\Delta\omega_c}{\omega_c} = -\frac{\Delta\gamma}{\gamma}$. This gives

$$\frac{\Delta\tilde{\omega}_{z,+}}{\tilde{\omega}_{z,+}} = \frac{1}{2}\frac{\Delta\omega_c}{\omega_c}, \tag{4.38}$$

which is the same slope as for one particle. If, on the other hand, one electron is de-excited and the other is excited, $m_1 = m_0$ and $m_2 = \gamma m_0$. Then, we multiply the z_1 equation by γ and add the two equations. Since $z_1 \approx z_2 \approx z_+$, the frequency of oscillation is

$$\tilde{\omega}_{z,+} = \sqrt{k(1+\gamma)/2\gamma m_0}. \tag{4.39}$$

We can approximate $z_1 \approx z_2 \approx z_+$ because the axial drive is half way between the two resonances (or they coincide if $m_1 = m_2 = \gamma m_0$). The variation in the axial frequency with respect to γ is $\frac{\Delta\tilde{\omega}_{z,\pm}}{\tilde{\omega}_{z,+}} = -\frac{1}{4}(\frac{2\gamma}{1+\gamma})\frac{\Delta\gamma}{\gamma}$. The variation of the cyclotron frequency remains $\frac{\Delta\omega_c}{\omega_c} = -\frac{\Delta\gamma}{\gamma}$. This gives (since $\gamma \approx 1$)

$$\frac{\Delta\tilde{\omega}_{z,+}}{\tilde{\omega}_{z,+}} = \frac{1}{4}\frac{\Delta\omega_c}{\omega_c}, \tag{4.40}$$

which is one half that for one particle. In this model, it is clear that when the system drops from the first branch to the second branch, the axial shift will be divided by two. This is observed.

When the equations of motion are subtracted to get an equation for the breathing modes, we get

$$\ddot{\tilde{z}}_- = -\frac{k}{\gamma m_0}\tilde{z}_- + \frac{q^2}{4\gamma m_0}\frac{(z_1 - z_2 + a)}{|z_1 - z_2 + a|^3}, \tag{4.41}$$

which is true for $m_1 = m_2$, and is approximately true for $m_1 = \gamma m_0, m_2 = m_0$. Setting the trap restoring force equal to minus the Coulomb repulsion force, we get that the effective spring constant for small oscillations is between 3k and k, depending on the soft core parameter, a.

When the excitation is obtained by sweeping the magnetic field, each of the branches is split into two, an upper branch and a lower branch. The lower branches seem to be more stable, while the upper branches are accessed when the field is swept back down. The axial frequency shift separation of the upper and lower branches on the first branch (20 Hz) is twice that of the separation on the second branch. The separation of the endpoints of the upper and lower branches on the cyclotron frequency axis is $\Delta\omega_c = 76.8$kHz. The endpoints for the upper and lower branches for the first branch and the second branch coincide.

Treatments of related cases are presented in [52, 8, 34, 5, 4]. The nonlinear motion of two particles in a trap displays transitions between order and chaos. This is evident only in the breathing mode since in the center of mass mode there is no non-linear Coulomb coupling. The two phases with different spatial trajectory

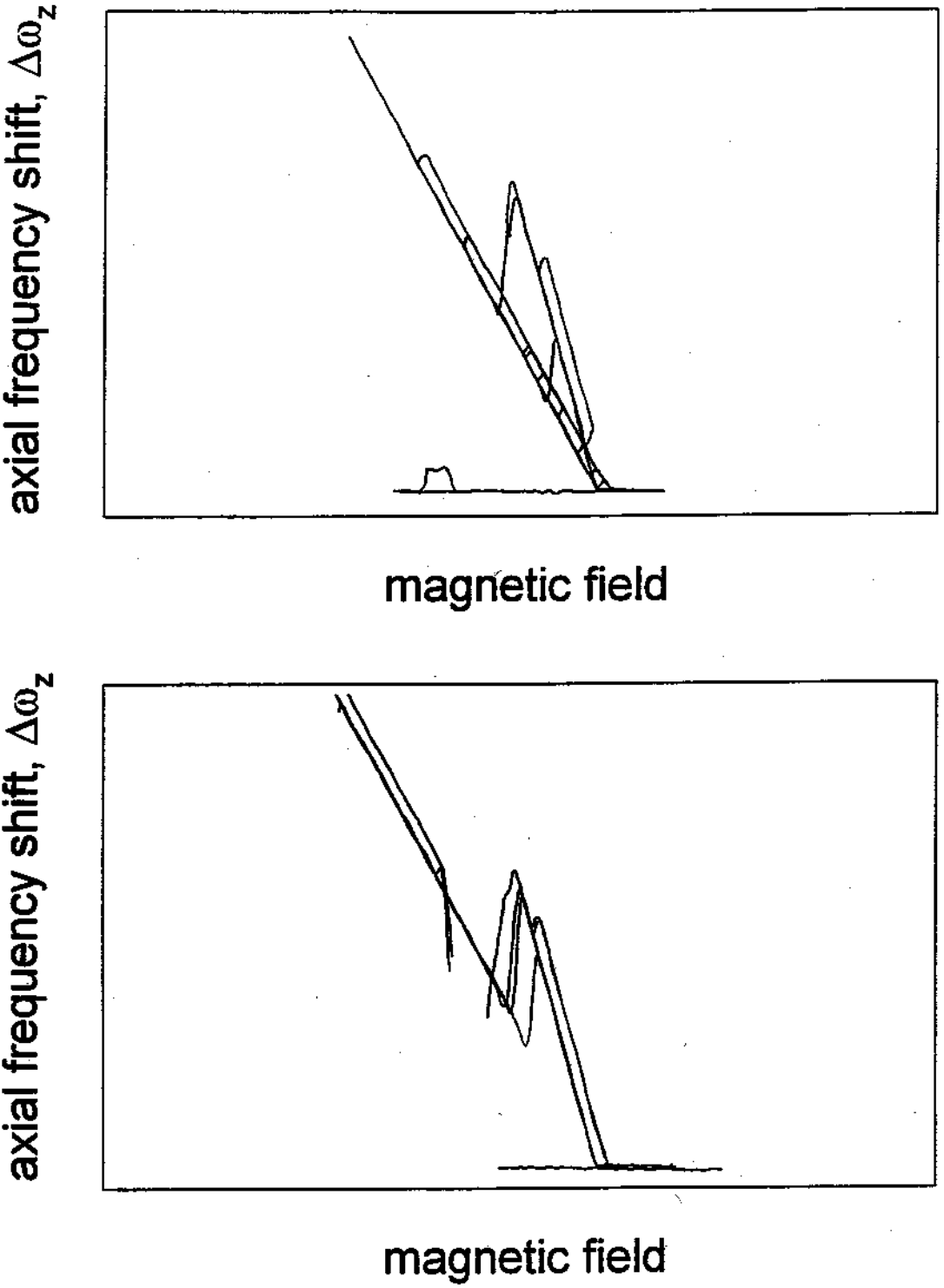

Figure 4.14: Two sets of observed two particle cyclotron resonances showing metastable upper branches that are accessed when the field is swept back down. During these traces the magnetic field is swept up and down several times. (The rectangular feature to the left of the top graph is a 10 Hz axial calibration shift.)

sets are perhaps coupled to the detected center of mass mode via electrostatic anharmonicities. These details for the two electron case have not yet been worked out.